BIBECHANA
Vol. 23, No. 2, April 2026, 146-156

ISSN 2091-0762 (Print), 2382-5340 (Online)
Journal homepage: http://nepjol.info/index.php/BIBECHANA
Publisher:Dept. of Phys., Mahendra Morang A. M. Campus (Tribhuvan University)Biratnagar

Thermodynamic and transport properties of Belinostat

Narayan Gautam[1,2], Deependra Awasthi[1], Shyam Prakash Khanal[1], Rajendra Prasad Koirala[1], Narayan Prasad Adhikari[1*]

[1] *Central Department of Physics, Tribhuvan University, Kirtipur, Nepal.*
[2] *Tri-Chandra Multiple Campus, Tribhuvan University, Kathmandu, Nepal.*

*Corresponding authors: Email: narayan.adhikari@cdp.tu.edu.np

Abstract

HDACs inhibitors, Belinostat inhibits class I HDACs, class II HDACs and class IV HDAC proteins activities. Antitumor activity of Belinostat is attributed to epigenetic control of gene expression and inhibition of protein repression. In this study, we have performed molecular dynamics simulation of Belinostat in water at 310 K temperature to investigate structural, thermodynamic and tranport properties. For the structural analysis, we have studied the radial distribution function (RDF). Thermodynamic integration (TI) and free energy perturbation (FEP) based methods: TI, TI-CUBIC, BAR and MBAR have been used to estimate solvation free energy. Our calculations show that Coulomb interactions has major contribution to the solvation free energy of Belinostat in water although both coulomb as well as vdW interaction contribute. Furthermore, we have estimated the sef-diffusion coefficient of both solute and solvent molecules with their binary diffusion coefficient from the slope of Mean Squared Displacement (MSD) versus time plot using Einstein's and Darken's relations respectively. Hydrogen bond and Solvent accessible surface area (SASA) analyses further support the strong hydration and structural stability of Belinostat in aqueous environment.

Keywords
HDACs inhibitors, Belinostat, solvation free energy, diffusion, SASA.

Article information
Manuscript received: February 3, 2026; Revised: April 27, 2026; Accepted: April 29, 2026
DOI https://doi.org/10.3126/bibechana.v23i2.92006

1 Introduction

Belinostat is a hydroxamic acid-based histone deacetylase (HDAC) inhibitor approved for the treatment of peripheral T-cell lymphoma (PTCL) [1]. PTCL represents a subgroup of non-Hodgkin lymphoma. As conventional chemotherapy often fail to render durable remission, there is a growing need for effective targeted therapeutic strategies for PTCL patients [2]. Belinostat has emerged as one of the promising therapeutic candidates to treat cancer. Chemically, Belinostat is known as ethyl $N-hydroxy-3-[3-(phenylsulfamoyl)phenyl]prop-2-enamide$ with molecular formula $C_{15}H_{14}N_2O_4S$ [3]. It contain a hydroxamic acid group capable of coordinating to the Zn^{2+} ion in the HDAC active site [4]. This zinc-binding property leads to inhibition of histone deacetylase enzymes which modulates the chromatin conformation and restores acetylation-dependent transcriptional activation of

tumor suppressor genes [5]. Due to this property, Belinostat is categorized as a HDAC inhibitor which target class I, class II and class IV HDAC enzymes [6]. The molecular structure of the Belinostat is shown in Figure 1(A).

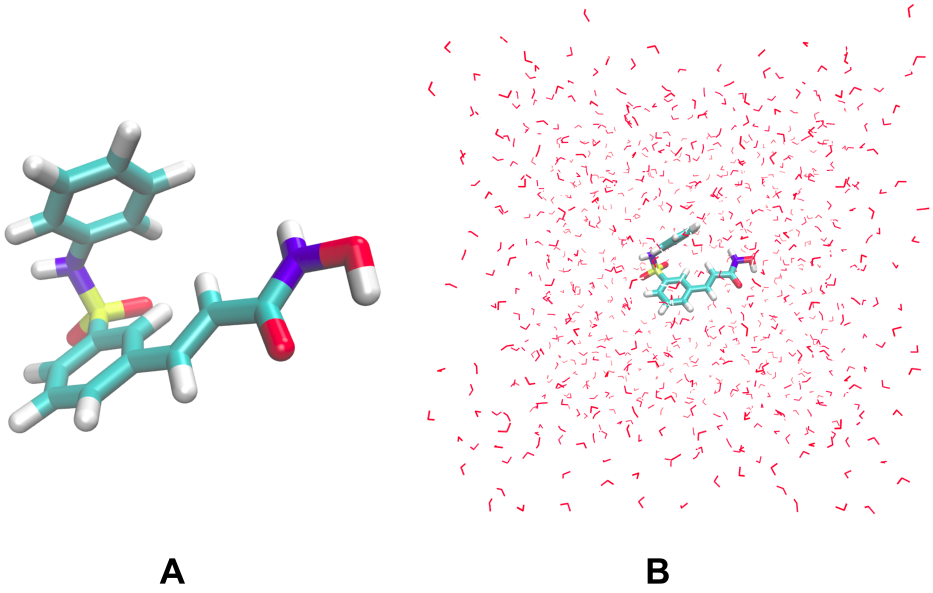

Figure 1: (A) Molecular structure of Belinostat, and (B) System of Belinostat prepared for the simulation

HDAC plays an important role in tumor survival, proliferation, differentiation, migration, and immune mechanisms [7]. Mutations in genes regulates DNA methylation and histone modifications that commonly occur in PTCL patients, leading to epigenetic disruption. This is especially responsive to HDAC inhibition [8]. HDAC inhibition makes Belinostat highly relevant not only clinically, but mechanistically as well, due to which it is a strong therapeutic candidate among targeted therapies for hematologic malignancies. The clinical significance and therapeutic importance of Belinostat were further supported by the results that demonstrated clinically meaningful responses in heavily pretreated PTCL patients with manageable toxicity [9]. Therefore, Belinostat is an important therapeutic molecule for clinical hematology and oncology research. Beyond clinical effects, the fundamental thermodynamic properties of Belinostat such as solvation behavior directly influence drug solubility, stability, protein-binding interactions, and membrane permeability [10]. Solvation-free energy is one of the essential thermodynamic parameters that determine the molecular accessibility of the drug in biological fluids and governs molecular partitioning events.

Accurate estimation of solvation-free energy is critical in predicting the energetics of drug-solvent interactions under physiological environments. Transport properties, such as self-diffusion, binary diffusion coefficient, and viscosity, are equally important as they determine the molecular mobility and interaction characteristics of drug molecules in solvent phases [11]. These parameters play key roles in determining dissolution rate, drug clearance, absorption behavior, intermolecular collision frequencies, and mass transport in biological systems. Therefore, a comprehensive understanding of both thermodynamic and transport parameters of Belinostat is essential not only from a pharmaceutical formulation point of view but also from a computational drug screening perspective. Molecular dynamics (MD) simulations are widely employed in computational physics for calculating free energy, transport properties, and predicting the stability of drug molecules in solvation environments [12].

Although, We have previously investigated the solvation free energy and transport properties of Panobinostat, HDAC inhibitor, using the classical MD simulation approach [13]. To the best of our knowledge, no prior molecular dynamics simulation study has investigated the solvation free energy and transport properties such as self-diffusion coefficient, binary diffusion coefficient, and viscosity of Belinostat in aqueous solution. While Belinostat has been studied experimentally as an HDAC inhibitor in biological contexts, its physicochemical behavior in water at the molecular level remains

unreported. The present work is therefore the first MD simulation study to comprehensively characterize the solvation thermodynamics and transport behavior of Belinostat in water at physiological temperature (310 K). These findings are expected to provide valuable insights into the physicochemical behavior of Belinostat in aqueous systems, contributing to rational drug design, optimization, and computational pharmacokinetic predictions.

2 Materials and Methods

2.1 Theoretical background

To study the macroscopic properties of a system from the analysis of trajectories of particles, molecular dynamics (MD) simulation is used which is based on the theory of statistical mechanics [14,15]. This technique simulates the motion of atoms and molecules. From the simulation results we explore the physical, chemical, and biological phenomena at the atomic level providing detailed insight into molecular structure, interactions, transport properties, and thermodynamic behavior [16]. It may be the efficient alternative of the experimental methods. Based on this approach, we performed MD simulations to investigate the solvation free energy, diffusion coefficient, and viscosity of Belinostat in aqueous solution, providing a molecular-level understanding of its stability, mobility, and physicochemical behavior.

2.1.1 Free Energy of Solvation

The free energy of solvation provides details into the stability, solubility, and interaction behavior of drug molecules in solution [17, 18]. Solvation free energy is crucial for understanding molecular processes such as binding thermodynamics, transport, and structural changes [19, 20]. Free energy calculations can be performed using several established methods. Free energy perturbation (FEP) method estimates the free energy difference between two thermodynamic states A and B with potential energy function U_A and U_B from ensemble averages of potential energy differences as [21]

$$\Delta F_{AB} = F_B - F_A = -k_B T \ln \langle \exp\left[-\beta\left(U_B - U_A\right)\right] \rangle_A \quad (1)$$

In the equation (1), $\langle \cdots \rangle_A$ represnts the average over the canonical ensemble of state A and $\beta = 1/(k_B T)$ with k_B represents Boltzmann constant. FEP is particularly effective for evaluating small perturbations in the system, such as solute-solvent interactions, and provides rapid and precise free energy estimates. Moreover, Thermodynamic Integration (TI) complements FEP by providing a continuous pathway between the two states. In TI, the free energy difference is obtained by integrating the ensemble-averaged derivative of the potential energy with respect to a coupling parameter λ that gradually transforms the system from state A ($\lambda = 0$) to state B ($\lambda = 1$) [21]

$$\Delta F_{AB} = \int_0^1 \left\langle \frac{\partial U(r,\lambda)}{\partial \lambda} \right\rangle_\lambda d\lambda \quad (2)$$

Here, $U(r, \lambda)$ is the potential energy as a function of atomic coordinates r and λ, commonly expressed using switching functions $f(\lambda)$ and $g(\lambda)$:

$$U(r,\lambda) = f(\lambda)U_A(r) + g(\lambda)U_B(r) \quad (3)$$

with $f(0) = 1$, $f(1) = 0$, $g(0) = 0$, and $g(1) = 1$. TI ensures transformation between the states, yielding free energy differences independent of the chosen pathway [22].

In this study, both FEP and TI were used to determine the solvation free energy of Belinostat in aqueous solution. This combination provides a comprehensive and accurate assessment of its thermodynamic stability.

2.1.2 Diffusion Coefficient

Diffusion of molecules is a fundamental transport process that influences the mobility and dissolution of drug molecules [23, 24]. The diffusion coefficient, D, quantifies this stochastic motion and can be determined from the mean square displacement (MSD) of particles using the Einstein relation [25]

$$D = \lim_{t\to\infty} \frac{\langle [r_\alpha(t+t_0) - r_\alpha(t_0)]^2 \rangle}{6t} \quad (4)$$

where,

- $r_\alpha(t+t_0)$: Position of particle α at time $t+t_0$,
- $r_\alpha(t_0)$: Position of the same particle at the initial time t_0, and
- $\langle [r_\alpha(t+t_0) - r_\alpha(t_0)]^2 \rangle$: Ensemble-averaged mean square displacement (MSD) over all particles.

2.2 Computational Details

We used CHARMM-GUI web server for the preparation of the system of Belinostat [16] by using the sdf file from PubChem Identifier: CID 6918638 [26]. To prepare the system we used Charmm36m force fields [27] and TIP3 [28] water model at pH 7.0. The Belinostat was solvated using the TIP3 water model in a cubic box and neutralized with 150 mM NaCl. The solvated and neutralized system of the Belinostat consists of 2707 atoms in a cubic simulation box which is shown in Figure 1(B). All

simulations were carried out at 310 K in under periodic boundary conditions (PBC) at 1 atm pressure using GROningen MAchine for Chemical Simulations (GROMACS) software package [29]. To remove van der Waals bad contact, we performed an energy minimization run using the steepest descent method [29].

2.2.1 Estimation of solvation free energy

To ensure a controlled and smooth decoupling of solute-solvent interactions, 21 discrete coupling parameter (λ) values were applied for both Coulombic and van der Waals interactions [30, 31]. The Coulombic λ values were defined as: λ_{Coulomb} = 0.00, 0.10, 0.20, 0.30, 0.40, 0.50, 0.60, 0.70, 0.80, 0.90, 1.0, 1.00, 1.00, 1.00, 1.00, 1.00, 1.00, 1.00, 1.00, 1.00 and 1.00 for Coulomb interaction; and λ_{vdW} = 0.00, 0.00, 0.00, 0.00, 0.00, 0.00, 0.00, 0.00, 0.00, 0.00,0.00, 0.10, 0.20, 0.30, 0.40, 0.50, 0.60, 0.70, 0.80, 0.90 and 1.00 for van der Waals interaction. The $\lambda = 0$ and $\lambda = 1$ states correspond to fully decoupled and fully interacting solute-solvent configurations, respectively, allowing precise estimation of the solvation free energy through integration of $\langle \partial U/\partial \lambda \rangle$ across all intermediate states.

We performed energy minimization run using steepest descent algorithm to eliminate steric clashes [29]. Then, equilibration was performed under NVT and NPT ensembles at 310 K and 1 atm pressure, respectively, with a time step of 2 fs [32]. Langevin thermostat is used to control the temperature, and pressures were maintained with a Parrinello-Rahman barostat (coupling time 1 ps, isothermal compressibility 4.5×10^{-5} bar^{-1} [33]. All bonds were constrained using the LINCS algorithm [34]. Long-range electrostatics interactions were estimated using the Particle Mesh Ewald (PME) method with a 1.2 nm real-space cutoff, while van der Waals interactions were truncated at the same distance [35]. Neighbor lists were updated every 20 steps, and soft-core potentials ($\alpha = 0.5$, $\sigma = 0.3$, $p = 1$) were applied to prevent singularities during decoupling [36]. Each λ-state was equilibrated for 2 ns, followed by a 5 ns production run. The solvation free energy of Belinostat was obtained by integrating the ensemble-averaged derivatives over all λ values, yielding a thermodynamically consistent and quantitatively accurate estimate of its hydration free energy.

2.2.2 Transport properties

To study the transport properties of Belinostat in aqueous solution, Belinostat molecule was solvated in a cubic box and performed all-atom MD simulations. Energy minimization was first carried out using the steepest descent algorithm to remove steric clashes. The systems were then equilibrated for 100 ns under an isothermal-isobaric (NPT) ensemble at 310 K and 1 atm for 500 ns of produciton run with a 2 fs time step using Leap-frog algorithms [35]. Long-range electrostatic interactions were handled with the Particle Mesh Ewald (PME) method, while short-range van der Waals and Coulomb interactions were truncated at 1.0 nm [37]. Initial velocities were assigned according to the Maxwell-Boltzmann distribution, and all bond lengths were constrained using the LINCS algorithm [34]. Thermal and barostatic control were maintained via a velocity-rescaling thermostat (coupling time 0.01 ps) and Berendsen barostat (coupling time 0.8 ps), respectively, under periodic boundary conditions [38, 39]. The mean square displacement (MSD) of Belinostat and surrounding water molecules was calculated from the equilibrated trajectories, and self-diffusion coefficients were determined using Einstein's relation. Only the initial portion of the trajectory was used for linear fitting to ensure high statistical reliability.

3 Results and discussion

Herein, we investigate the thermodynamic and transport properties such as solvation free energy, and diffusion coefficients of Belinostat molecule in aqueous enviroment.

3.1 Free Energy of Solvation

The solvation free energy of Belinostat was determined using thermodynamic integration (TI), cubic-spline TI (TI-CUBIC), and free-energy perturbation (FEP), based Bennett Acceptance Ratio (BAR) and Multistate Bennett Acceptance Ratio (MBAR) methods to ensure accurate and statistically consistent estimation of the free-energy profile. In TI and TI-CUBIC calculations, the coupling parameter λ was varied from 0 to 1 to construct a series of intermediate, non-physical thermodynamic states between the fully coupled ($\lambda = 0$) and fully decoupled ($\lambda = 1$) states. Trapezoidal and cubic-spline rules are used to evaluate $\left\langle \frac{\partial U}{\partial \lambda} \right\rangle_{\lambda}$ across the alchemical analysis. The Coulombic interactions were first gradually switched off while retaining full van der Waals (vdW) coupling, followed by the decoupling of vdW interactions. Figure 2(A) shows the corresponding energy derivatives, where the red color shows the electrostatic contribution and the green color represents the van der Waals (vdW) contribution to the solvation free energy of the Belinostat molecule.

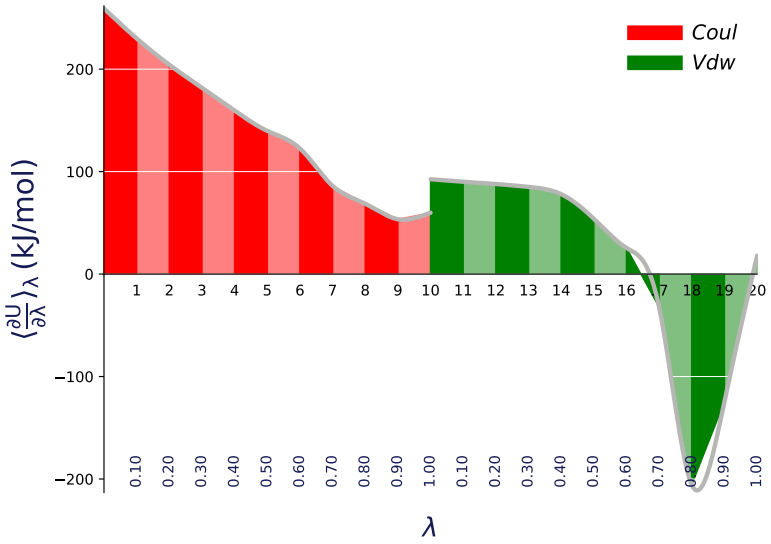

Figure 2: (A) Variation of $\langle \frac{\partial U}{\partial \lambda} \rangle_\lambda$ with λ for Belinostat taking TIP3P water model as solvent at temperature 310 K.

The sharp increase in the coulombic term at higher value of λ shows the activation of electrostatic interactions between Belinostat and the water. On the other hand, the vdW contribution increases slowly and uniformly as the Belinostat creates space in the solvent and develops favorable dispersion forces. BAR and MBAR values are in close agreement with TI and TI-CUBIC derived values which validate the thermodynamic predictions. These results establish that the solvation thermodynamics of Belinostat are dominated by electrostatic interactions, with vdW forces serving as secondary stabilizing contributions. The Coulombic measurements reflects the intrinsic polarity of Belinostat, indicating that its hydration is governed primarily by solvent reorganization around charged and polar regions. This thermodynamic profile has direct implications for its aqueous stability in biological systems. The estimated values of solvation free energy of Belinostat molecules in water at 310 K using different methods are presented in Table 1.

The time series plots demonstrate that the free energy calculations converge after a fraction of the simulation time, with the forward and reverse ΔG values closely agreed after the initial hysteresis effect as shown in Figure 2(B). This confirms that the free energy estimates reach equilibrium, validating the reliability of the computed solvation free energy.

Hydrogen Bond Analysis

Hydrogen bond play am important role in stabilizing bimolecular systems. Molecular dynamics simulation of Belinostat molecule shows the energetically favorable interactions between its polar functional groups and surrounding water molecules. We have analyzed the hydrogen bonds between Belinostat and water molecules using trajectory after 5 ns production for initial i.e., coupling state represented by $\lambda = 0$. As shown in Figure 3(A), during the 5 ns simulation, Belinostat form the consistent stable hydrogen-bond network.

Table 1: Estimated values of solvation free energy of Belinoststst in water at 310 K using different methods.

States	TI (kJ/mol)	TI-CUBIC (kJ/mol)	BAR (kJ/mol)	MBAR (kJ/mol)
$0 \rightarrow 1$	24.45 ± 0.02	24.44 ± 0.02	24.43 ± 0.02	24.41 ± 0.02
$1 \rightarrow 2$	21.71 ± 0.02	21.68 ± 0.02	21.69 ± 0.02	21.71 ± 0.02
$2 \rightarrow 3$	19.30 ± 0.02	19.29 ± 0.02	19.29 ± 0.02	19.29 ± 0.02
$3 \rightarrow 4$	17.07 ± 0.02	17.07 ± 0.02	17.04 ± 0.02	17.04 ± 0.01
$4 \rightarrow 5$	14.97 ± 0.02	14.90 ± 0.02	14.95 ± 0.02	14.79 ± 0.01
$5 \rightarrow 6$	13.12 ± 0.02	13.24 ± 0.02	13.11 ± 0.02	12.30 ± 0.01
$6 \rightarrow 7$	10.43 ± 0.01	10.43 ± 0.02	9.76 ± 0.01	9.84 ± 0.01
$7 \rightarrow 8$	7.74 ± 0.10	7.62 ± 0.11	7.72 ± 0.00	7.95 ± 0.00
$8 \rightarrow 9$	6.11 ± 0.10	6.03 ± 0.11	5.97 ± 0.02	6.59 ± 0.00
$9 \rightarrow 10$	5.07 ± 0.01	5.52 ± 0.03	6.28 ± 0.01	5.45 ± 0.01
$10 \rightarrow 11$	9.13 ± 0.01	9.13 ± 0.02	9.13 ± 0.01	9.16 ± 0.01
$11 \rightarrow 12$	8.90 ± 0.02	8.91 ± 0.02	8.92 ± 0.02	9.03 ± 0.01
$12 \rightarrow 13$	8.65 ± 0.02	8.66 ± 0.02	8.71 ± 0.02	8.75 ± 0.01
$13 \rightarrow 14$	8.15 ± 0.02	8.25 ± 0.02	8.19 ± 0.02	8.14 ± 0.02
$14 \rightarrow 15$	6.60 ± 0.02	6.73 ± 0.03	6.64 ± 0.03	6.64 ± 0.03
$15 \rightarrow 16$	3.98 ± 0.04	3.88 ± 0.04	4.11 ± 0.04	4.13 ± 0.04
$16 \rightarrow 17$	−0.33 ± 0.07	0.77 ± 0.09	0.21 ± 0.08	0.20 ± 0.08
$17 \rightarrow 18$	−11.89 ± 0.12	−12.58 ± 0.13	−12.06 ± 0.25	−12.06 ± 0.25
$18 \rightarrow 19$	−16.51 ± 0.10	−18.34 ± 0.12	−18.11 ± 0.09	−18.33 ± 0.09
$19 \rightarrow 20$	−5.34 ± 0.03	−5.24 ± 0.04	−5.37 ± 0.03	−5.37 ± 0.02
Coulomb:	140.56 ± 0.21	140.21 ± 0.20	140.25 ± 0.05	139.35 ± 0.06
vdWaals:	11.34 ± 0.26	10.17 ± 0.26	10.37 ± 0.28	10.30 ± 0.31
TOTAL:	151.91 ± 0.33	150.38 ± 0.33	150.62 ± 0.29	149.65 ± 0.31

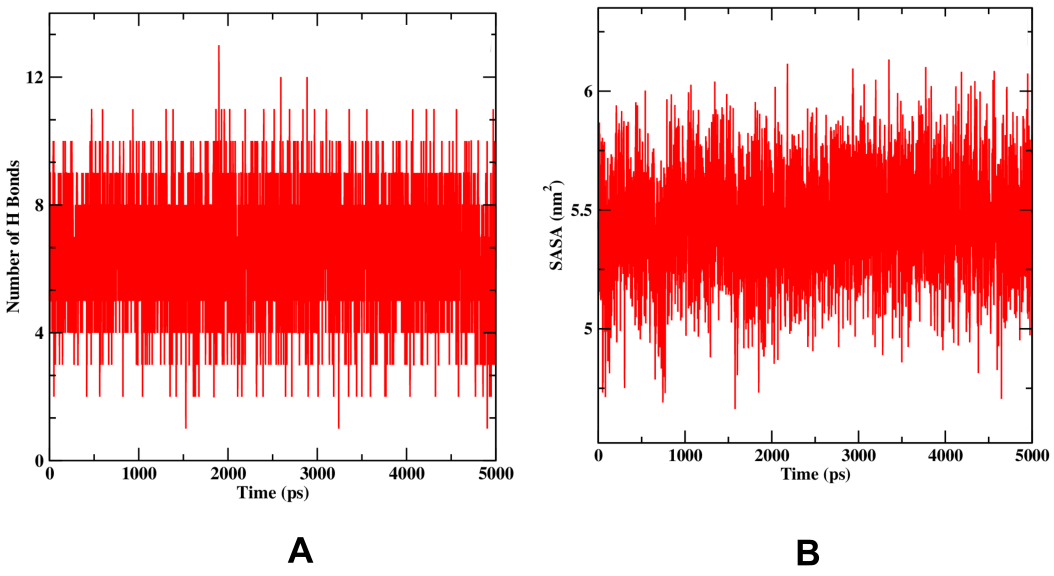

Figure 3: (A)The variation in the number of hydrogen bonds between the Belinostat and TIP3P water molecules at 310 K for the initial state at $\lambda = 0$, and (B) Solvent Accessible Surface Area of Belinostat in water.

The stable hydrogen-bonding pattern provides favorable interaction between the Belinostat and water that underscore its central role in thermodynamic behavior. Consistent hydrogen-bond formation reduces fluctuations in solvation energetics, enhancing the reliability of free-energy calculations. The observed hydration dynamics also suggest that Belinostat will maintain robust solvation behavior across different aqueous environments, ensuring structural integrity under varying conditions. Furthermore, we have also investigated the transport properties of the Belinostat in water focusing on

diffusion coefficient and shear viscosity.

3.2 Solvent Accessible Surface Area (SASA)

Solvent accessible surface area (SASA) represents total surface area of molecule that is directly exposed to the solvent. As shown in Figure 3(B), Belinostat exhibits a stable SASA that ranges approximately $5.0-6.0\,nm^2$ across the entire trajectory of the simulation, with only minor thermal fluctuations. This smooth and uniform profile of SASA measurements of Belinostat indicate that its polar components remain consistently hydrated.

3.3 Transport Properties

We have estimated the self diffusion coefficient of the Belinostat as solute molecules and water, as well as their binary diffusion coefficient at 310 K temperature.

Diffusion Coefficients

The mean-square displacement (MSD) of Belinostat is presented in Figure 4 that exhibits a smoothly increasing logarithmic trend across the full molecular dynamics simulation. The MSD curve rises steeply during the initial picoseconds, corresponding to rapid local relaxation dynamics, and subsequently transitions into a stable, near-linear progression on the log-log axes. The MSD curve shows that Belinostat remains dynamically unrestricted in the aqueous environment.

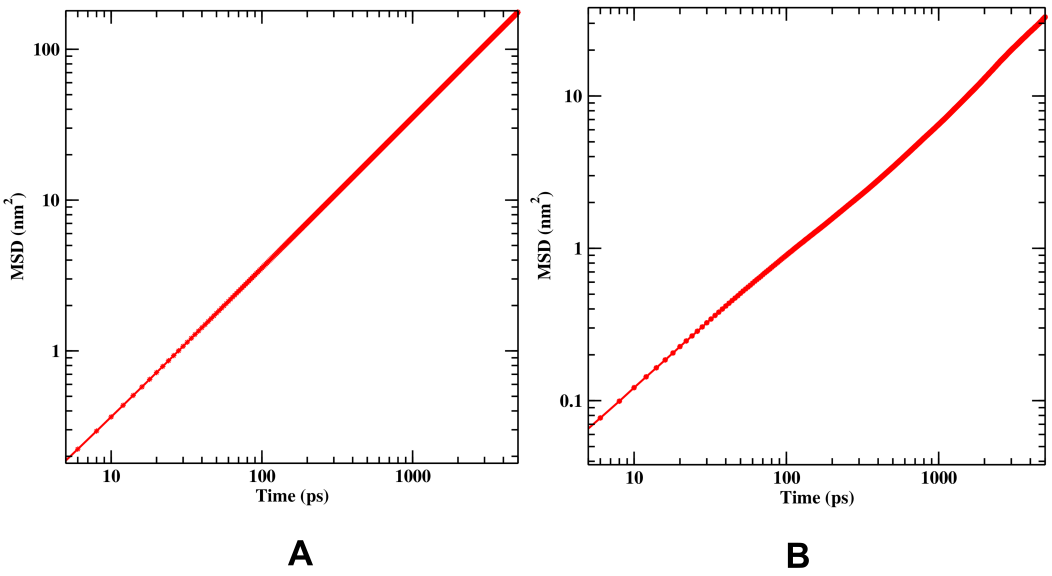

Figure 4: MSD versus time plot in logarithmic scale for (A) Water, and (B) Belinostat at temperature 310 K.

The mean-square displacement profile for water, as shown in the figure 4 (A), exhibits a smooth and continuously increasing logarithmic trend of homogeneous solvent. From the long-timescale behavior visible in the figure 4 (B), Belinostat clearly attains a well-defined diffusive regime. The MSD rises sharply at short times due to rapid motions of water molecules and subsequently transitions into a stable, uniform slope across the intermediate and long-time regions of the log–log plot [40]. The plot shows that the system attains a well-defined diffusive regime, reflecting the intrinsic dynamical behavior of bulk liquid water. This consistently progressing MSD trajectory demonstrates that the simulation adequately captures the physical mobility of the solvent and provides a robust basis for determining the self-diffusion coefficient with high reliability [41].

The MSD profiles of Belinostat and water show smooth logarithmic increases, reflecting well-defined diffusive behavior. Belinostat does not exhibits a perfect slope that may be due to solvation, molecular reorientation, and intermolecular interactions, while water shows rapid and uniform diffusion characteristic of bulk solvent molecules. Both MSD profiles attain appropriate diffusive regimes that validate the physical meaning and reliability of the self-diffusion coefficients reported in the Table 2.

The estimated self-diffusion coefficient of water (5.86×10^{-9} m^2/s) is in close agreement with the experimental reference value of 7.05×10^{-9} m^2/s [42]. The reliability of this study is further supported by our previous MD study on Panobinostat, a structurally related HDAC inhibitor, where the same computational protocol yielded a water self-diffusion coefficient of 6.75×10^{-9} m^2/s with a percentage error of 4.26% against the same reference [13]. The self-diffusion coefficient of Belinostat (1.20×10^{-9} m^2/s) is approximately 4.9 times lower than that of water, consistent with the larger molecular size and reduced mobility of the drug molecule in aqueous solution. The binary diffusion coefficient of Belinostat in water is estimated to be 1.236×10^{-9} m^2/s.

Table 2: Self diffusion coefficients of Belinostat and water molecules as well as their binary diffusion coefficient at 310 K temperature.

Diffusion coefficient ($\times 10^{-9}$ m^2/s)			
Self			Binary
Belinostat	Water		
Estimated	Estimated	Ref. [42]	Estimated
1.20	5.86	7.05	1.236

Table 2 shows that Belinostat has a much lower self-diffusion coefficient than water, and its binary diffusion in dilute solution closely matches with its self-diffusion. This indicates that Belinostat diffuses slowly due to its size and hydrogen-bonding interactions, confirming the reliability of the MD simulations.

3.4 Structural Analysis

The structural analysis of the system can studied through the radial distribution function (RDF) $g_{XY}(r)$ that provides the structural information about the distribution of molecules around another molecule [43, 44]. The RDF between the molecule (X) at center and the surrounding molecules (Y) as a function of intermolecular distance r is defined as [29]

$$g_{XY}(r) = \frac{\langle \rho_Y(r) \rangle}{\langle \rho_Y \rangle_{\text{local}}} = \frac{1}{\langle \rho_Y \rangle_{\text{local}}} \frac{1}{N_X} \sum_{i \in X} \sum_{j \in Y} \frac{\delta(r_{ij} - r)}{4\pi r^2} \quad (5)$$

In the equation 5, the terms $\rho_Y(r)$ and $\langle \rho_Y \rangle$ gives the particle density of type Y at a distance r around particles X, and particle density of type Y averaged over all the spheres around particles X respectively. Figures 5(A) and 5(B) represents the RDF between the spatial orientation between the oxygen atoms of water molecules and oxygen atom of Belinostat with the surrounding water molecules, respectively.

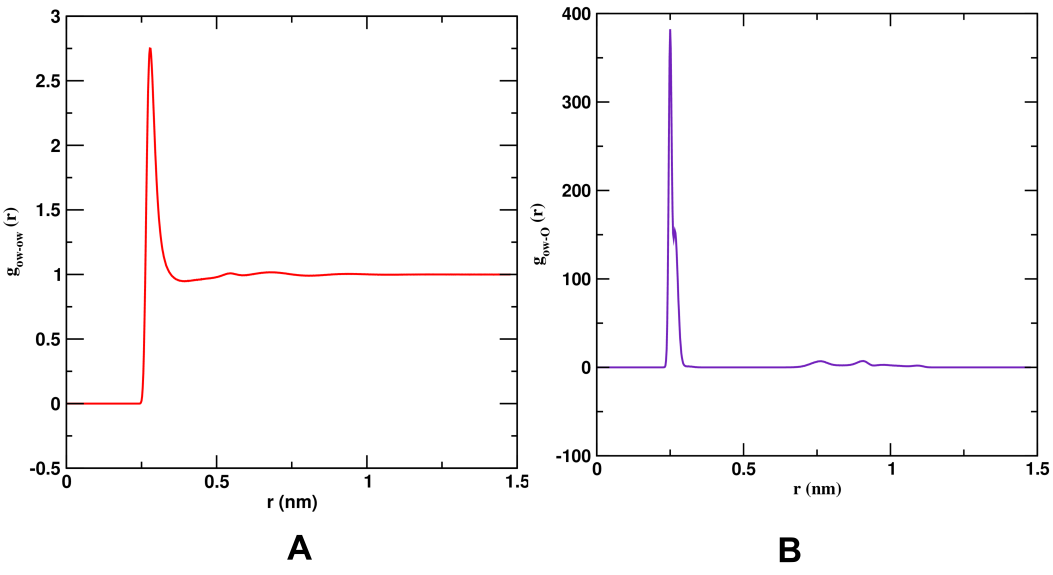

Figure 5: (A)Radial distribution function (RDF) between oxygen atoms of water molecules, and (B) oxygen atom of Belinostat and water molecules

In Figure 5(A), the RDF curves for oxygen-oxygen of water molecules with a well-defined first coordination peak observed near $r = 0.8$ nm. Figure 5(B) shows the RDF curve for oxygen atom of water molecules and oxygen atom of Belinostat molecule with a first coordination peak observed near $r = 0.25$ nm.

This suggests the strong solvation tendency of the oxygen atoms of Belinostat in water. A sharp and intense first peak centered around $r = 0.25$ nm ($g(r) \approx 380$) corresponds to the first hydration shell, highlighting strong hydrogen-bonding interactions between the polar oxygen sites and the hydrogen atoms of water. A secondary peak around $r = 0.70$ nm indicates the presence of a second, less ordered solvation layer.

4 Conclusions

We have performed molecular dynamic study to understand solvation mechanism and diffusion process of Belinostat in water through the estimation of solvation free energy and diffusion coefficient. System under study was modeled using charmm36m force field and TIP3 water model. The solvation free energy of Belinostat molecule in water have been estimated at 310 K temperature using TI and FEP based methods. The estimated values of solvation free energy using TI, TI-CUBIC, BAR and MBAR methods are 151.91 ± 0.33, 150.38 ± 0.33, 150.62 ± 0.29, & 149.65 ± 0.31 in kJ/mol respectively. The solvation free energy estimated using different methods are in close agreement ensure convergence of the calculations. We have also analyzed the individual contribution of Coulomb and vdW interactions to the total solvation free energy; and our results show that Coulomb interaction has major contribution on solvation free energy, ≈ 140 kJ/mol. Approximately six hydrogen bonds has been observed throughout simulation; and the hydrogen bonding network greatly impacts on solvation free energy and improves the stability of solvation. Moreover, to understand the solute-solvent interaction, we have also analyzed the SASA of the solute molecules which is nearly 5.2 nm^2. Furthermore, to understand the diffusion of HDACs inhibitors, self diffusion coefficient of both solute and solvent molecules as well as their binary diffuion coefficient have been estimtaed at 310 K temperature through the analysis of MSD followed by the particles using Einstein's and Darken's relation respectively. These results provide the valuable insights of solvation free energy and offer important information for the development of new HDACs inhibitors including improvement of Belinostat. Future work could explore the effect of temperature variations on these parameters for the comparative analysis with structurally similar molecules.

Acknowledgments

NG acknowledges the PhD Research Grant (Regular) from Nepal Academy of Science and Technology (NAST).

Author contributions

NG designed the project. NPA supervised the project. NG performed the MD simulations and analyzed the data. All authors contributed to the data analysis and interpretation. NG wrote the manuscript. SPK, RPK and NPA contributed to manuscript editing.

Disclosure statement

There is no conflict of interest

References

[1] O'Connor OA, Horwitz S, Masszi T, Van Hoof A, Brown P, Doorduijn J, et al. Belinostat in Patients with Relapsed or Refractory Peripheral T-Cell Lymphoma: Results of the Pivotal Phase II BELIEF (CLN-19) Study. Journal of Clinical Oncology. 2015;33(23):2492-9.

[2] Savage KJ. Peripheral T-Cell Lymphomas. Blood Reviews. 2007;21(4):201-16.

[3] Plumb JA, Finn PW, Williams RJ, Bandara MJ, Romero MR, Watkins CJ, et al. Pharmacodynamic Response and Inhibition of Growth of Human Tumor Xenografts by the Novel Histone Deacetylase Inhibitor PXD101. Molecular Cancer Therapeutics. 2003;2(8):721-8.

[4] Vigushin DM, Ali S, Pace PE, Mirsaidi N, Ito K, Adcock I, et al. Trichostatin A is a Histone Deacetylase Inhibitor with Potent Antitumor Activity Against Breast Cancer in Vivo. Clinical Cancer Research. 2001;7(4):971-6.

[5] Karagiannis D, Rampias T. HDAC Inhibitors: Dissecting Mechanisms of Action to Counter Tumor Heterogeneity. Cancers. 2021;13(14):3575.

[6] Poole RM. Belinostat: First Global Approval. Drugs. 2014;74(13):1543-54.

[7] Couronné L, Bastard C, Bernard OA. TET2 and DNMT3A Mutations in Human T-Cell Lymphoma. New England Journal of Medicine. 2012;366(1):95-6.

[8] Zhang P, Zhang M. Epigenetic Alterations and Advancement of Treatment in Peripheral T-Cell Lymphoma. Clinical Epigenetics. 2020;12(1):169.

[9] Reimer P, Chawla S. Long-Term Complete Remission with Belinostat in a Patient with Chemotherapy Refractory Peripheral T-Cell

Lymphoma. Journal of Hematology & Oncology. 2013;6(1):69.

[10] Liu JY, Yen CH, Lin YF, Feng YH, Fang YP. Improving the Thrombocytopenia Adverse Reaction of Belinostat Using Human Serum Albumin Nanoparticles. International Journal of Nanomedicine. 2024:10785-800.

[11] Miyamoto S, Shimono K. Molecular Modeling to Estimate the Diffusion Coefficients of Drugs and Other Small Molecules. Molecules. 2020;25(22):5340.

[12] Durrant JD, McCammon JA. Molecular Dynamics Simulations and Drug Discovery. BMC Biology. 2011;9(1):71.

[13] Gautam N, Awasthi D, Khanal SP, Koirala RP, Adhikari NP. Thermodynamic Behavior, Diffusion Mechanisms and Structural Properties of Panobinostat in Water. Journal of Institute of Science and Technology. 2025;30(2):93-104.

[14] Karplus M, Petsko GA. Molecular Dynamics Simulations in Biology. Nature. 1990;347(6294):631-9.

[15] Allen MP, Tildesley DJ. Computer Simulation of Liquids. Oxford University Press; 1987.

[16] Dror RO, Jensen M, Borhani DW, Shaw DE. Exploring Atomic Resolution Physiology on a Femtosecond to Millisecond Timescale Using Molecular Dynamics Simulations. Journal of General Physiology. 2010;135(6):555-62.

[17] Choi H, Kang H, Park H. New Solvation Free Energy Function Comprising Intermolecular Solvation and Intramolecular Self-Solvation Terms. Journal of Cheminformatics. 2013;5(1):8.

[18] Matos GDR, Kyu DY, Loeffler HH, Chodera JD, Shirts MR, Mobley DL. Approaches for Calculating Solvation Free Energies and Enthalpies Demonstrated with an Update of the FreeSolv Database. Journal of Chemical & Engineering Data. 2017;62(5):1559-69.

[19] Friston K, Kilner J, Harrison L. A Free Energy Principle for the Brain. Journal of Physiology-Paris. 2006;100(1–3):70-87.

[20] Kirkwood JG. Statistical Mechanics of Fluid Mixtures. The Journal of Chemical Physics. 1935;3(5):300-13.

[21] Tuckerman ME. Statistical Mechanics: Theory and Molecular Simulation. Oxford University Press; 2023.

[22] Mitchell MJ, McCammon JA. Free Energy Difference Calculations by Thermodynamic Integration: Difficulties in Obtaining a Precise Value. Journal of Computational Chemistry. 1991;12(2):271-5.

[23] Rapaport DC. The Art of Molecular Dynamics Simulation. Cambridge University Press; 2004.

[24] Bhandari D, Adhikari NP. Molecular Dynamics Study of Diffusion of Krypton in Water at Different Temperatures. International Journal of Modern Physics B. 2016;30(11):1650064.

[25] Einstein A. Investigations on the Theory of the Brownian Movement. Courier Corporation; 1956.

[26] Kim S, Cheng CJ, Gindulyte A, He J, He S, Li Q, et al. PubChem 2025 Update. Nucleic Acids Research. 2025;53(D1):D1516-25.

[27] Huang J, Rauscher S, Nawrocki G, Ran T, Feig M, de Groot BL, et al. CHARMM36m: An Improved Force Field for Folded and Intrinsically Disordered Proteins. Nature Methods. 2017;14(1):71-3.

[28] Mark P, Nilsson L. Structure and Dynamics of the TIP3P, SPC, and SPC/E Water Models at 298 K. The Journal of Physical Chemistry A. 2001;105(43):9954-60.

[29] Van Der Spoel D, Lindahl E, Hess B, Groenhof G, Mark AE, Berendsen HJC. GROMACS: Fast, Flexible, and Free. Journal of Computational Chemistry. 2005;26(16):1701-18.

[30] Khanal SP, Adhikari NP. Thermodynamic and Transport Properties of Amoxicillin. Journal of Molecular Liquids. 2022;354:118865.

[31] Bhatta T, Khanal P, Khanal SP, Adhikari NP. Thermodynamics and Transport Properties of Valine and Cysteine Peptides in Water. Journal of Molecular Liquids. 2023;376:121472.

[32] Koirala RP, Bhusal HP, Khanal SP, Adhikari NP. Effect of Temperature on Transport Properties of Cysteine in Water. AIP Advances. 2020;10(2).

[33] Parrinello M, Rahman A. Polymorphic Transitions in Single Crystals: A New Molecular Dynamics Method. Journal of Applied Physics. 1981;52(12):7182-90.

[34] Hess B, Bekker H, Berendsen HJC, Fraaije JGEM. LINCS: A Linear Constraint Solver for Molecular Simulations. Journal of Computational Chemistry. 1997;18(12):1463-72.

[35] Hess B, van Der Spoel D, Lindahl E, et al.. GROMACS User Manual Version 4.5.4. Netherland; 2010.

[36] Steinbrecher T, Joung I, Case DA. Soft-Core Potentials in Thermodynamic Integration: Comparing One- and Two-Step Transformations. Journal of Computational Chemistry. 2011;32(15):3253-63.

[37] Essmann U, Perera L, Berkowitz ML, Darden T, Lee H, Pedersen LG. A Smooth Particle Mesh Ewald Method. The Journal of Chemical Physics. 1995;103(19):8577-93.

[38] Bussi G, Donadio D, Parrinello M. Canonical Sampling Through Velocity Rescaling. The Journal of Chemical Physics. 2007;126(1).

[39] Berendsen HJC, van Postma JPM, Van Gunsteren WF, DiNola ARHJ, Haak JR. Molecular Dynamics with Coupling to an External Bath. The Journal of Chemical Physics. 1984;81(8):3684-90.

[40] Caspi A, Granek R, Elbaum M. Enhanced Diffusion in Active Intracellular Transport. Physical Review Letters. 2000;85(26):5655.

[41] Metzler R, Klafter J. The Random Walk's Guide to Anomalous Diffusion: A Fractional Dynamics Approach. Physics Reports. 2000;339(1):1-77.

[42] Rosas Jimenez JG, Fábián B, Hummer G. Faster Sampling in Molecular Dynamics Simulations with TIP3P-F Water. Journal of Chemical Theory and Computation. 2024;20(24):11068-81.

[43] Allen MP, Tildesley DJ. Computer Simulation of Liquids. Oxford University Press; 2017.

[44] Hansen JP, McDonald IR. Theory of Simple Liquids: With Applications to Soft Matter. Academic Press; 2013.